Available online at www.sciencedirect.com
ScienceDirect
Ceramics International 37 (2011) 2255–2261
CERAMICS INTERNATIONAL
www.elsevier.com/locate/ceramint

Mechanical behavior and failure mechanisms of boron carbide based three-layered laminates with weak interfaces

Mykola Lugovy [a], Viktor Slyunyayev [a], Vladimir Subbotin [a], Fei Liang [b], Jihua Gou [b], Nina Orlovskaya [b,*], Thomas Graule [c], Jakob Kuebler [c]

[a] *Institute for Problems of Materials Science, 3 Krzhizhanivskii Str., 03142 Kyiv, Ukraine*
[b] *University of Central Florida, Orlando, 4000 Central Florida Blvd., Orlando, FL 32816, USA*
[c] *Empa, Ueberlandstrasse 129, 8600 Duebendorf, Switzerland*

Received 30 August 2010; received in revised form 28 February 2011; accepted 8 March 2011
Available online 14 April 2011

Abstract

The effect of weak interfaces on failure mechanisms of a three-layered composite was studied. Three-layered $B_4C/B_4C–C_{nanofibers}$ laminates have been produced using a hot pressing technique. The laminates were designed with thick (~2.6 mm) outer layers of B_4C and a thin (~90 μm) center layer of B_4C–70 wt.% $C_{nanofibers}$. Based on the difference in coefficients of thermal expansion and Young's moduli of the pure B_4C and B_4C–70 wt.% $C_{nanofibers}$ layers, it was estimated that low tensile thermal residual stress with a magnitude of 11.3 ± 2.5 MPa was developed in the thick B_4C outer layers, and compressive residual stress with a magnitude of 455.7 ± 5 MPa was developed in the thin central B_4C–70 wt.% $C_{nanofibers}$ layer. The apparent fracture toughness of laminates was measured and based on the estimated fracture toughness values, a threshold stress was calculated.

Keywords: Laminate; Ceramics; Fracture toughness; Residual stress

1. Introduction

It was established that the toughness of brittle ceramics can be significantly increased by creating weak interfaces in a ceramic composite [1–4]. This idea was carefully explored on different materials such as SiC and B_4C, by incorporating fibers inside the brittle ceramic matrix [5,6]. Technologically, it is not easy to incorporate these fibers or fiber bundles into ceramics since there is a big misfit of thermal expansions and Young moduli between the two components, which can cause cracking that easily degrades all properties of the composites. The problem encountered in fiber reinforced ceramic composites was how to incorporate fibers that produce weak interfaces in a strong ceramic matrix that are weak enough to deflect propagating cracks yet strong enough to maintain the mechanical integrity of the whole ceramic composite. Hot pressing is a very promising technique when it comes to densifying covalent ceramics that are difficult to sinter. It is broadly used to fully densify both SiC and B_4C, where strong covalent bonds are prevailing and very difficult to sinter without the application of high temperatures up to 2200 °C and pressure up to 50 MPa simultaneously. However, while making and densifying B_4C fiber reinforced composites is a difficult task to accomplish, the design and processing of multilayered B_4C based composites that incorporate carbon nanofibers is one of the most feasible options to pursue.

One of the approaches to produce ceramic composites with weak yet efficient interfaces was proposed by Clegg [7]. In his approach, the SiC sheets coated with graphite were compacted together by pressureless sintering in order to produce laminate ceramics. The catastrophic failure of such composites was prevented by the deflection of the propagating crack into the interfaces while the apparent fracture toughness was increased from 3.6 MPa $m^{1/2}$ to 17.7 MPa $m^{1/2}$, along with an increase in work required to break the sample. Therefore, the concept of improving the resistance to crack growth of an inherently brittle material by having a series of laminae separated by weak interfaces capable of deflecting cracks is well established [8].

* Corresponding author.
E-mail address: norlovsk@mail.ucf.edu (N. Orlovskaya).

0272-8842/$36.00
doi:10.1016/j.ceramint.2011.03.065

The basic requirement is that as a crack propagates through the base material, it should be deflected at weak interfaces oriented transversely to the main crack propagation direction. It is expected that the toughness of the material will be optimized when the interfaces are weak enough to ensure that crack deflection consistently occurs.

The approach [9] to develop three-layered B_4C–SiC based composites with strong interfaces was used to design B_4C/B_4C–SiC laminates. A significant increase of the apparent fracture toughness from 2.8 to 3.3 MPa $m^{1/2}$ for pure B_4C to 7.42 ± 0.82 MPa $m^{1/2}$ for three-layered B_4C/B_4C–SiC composite was reported [10]. The current work is an attempt to develop three-layered B_4C based composites where weak interfaces are incorporated into a brittle B_4C matrix by designing the middle layer with B_4C mixed with carbon nanofibers. Such a B_4C–$C_{nanofibers}$ layer has a lower coefficient of thermal expansion in comparison with pure B_4C ceramics, along with more difficult densification of carbon material, which should give the required result – the creation of weak interfaces inside B_4C ceramics.

Such a possibility of weak interfaces creation using a thin layer of B_4C–70 wt.% $C_{nanofibers}$ is investigated. The effect of the residual stress on the apparent fracture toughness and crack growth in B_4C-based layered composites with weak interfaces is also analyzed in this study. Special attention is paid to the study of the weak interfaces effect on the failure mechanism of the laminate.

2. Manufacturing of three-layered ceramics

Three-layered laminates with thick outer layers of pure B_4C and a thin inner layer of carbon nanofiber paper as well as pure B_4C specimens were fabricated. The main manufacturing steps for the laminates included the grinding of raw powders, stacking B_4C powders and carbon nanofiber paper together to form the three-layered structure, and hot pressing the laminates. Only grinding the raw powders and hot pressing were done for pure B_4C specimens. The hot pressing conditions were as follows: a heating rate of 100 °C/min, a hot pressing temperature of 2150 °C, a pressure of 30 MPa, and a dwell time of 1 h. As a result, dense laminate samples (98–99% relative density) and pure boron carbide specimens were obtained and further machined into 3 mm × 5 mm × 45 mm bars for 4 point bending and fracture toughness experiments.

Carbon nanofiber paper was made of vapor grown carbon nanofibers (Polygraf III, PR-25-HHT) and B_4C powders. The PR-25-HHT nanofibers were supplied by Applied Sciences, Inc. (ASI, Cedarville, Ohio, USA) with a diameter of ~80 nm and a length of 30–100 μm. They were thermally treated over 1200 °C in an inert atmosphere, in order to have a highly ordered graphitic surface, low surface energy, low iron content, and a small diameter.

The heat-treated carbon nanofibers were dispersed into distilled water with an aid of the surfactant Triton-X100. The mixture was sonicated with a high intensity sonicator (600-W Sonicator 3000 supplied by Misonix Inc., New York, USA) for 30 min at a power level of 30–50 W to form a suspension. The B_4C powders were dispersed into water through the water boiling process. The suspension of nanofibers was then mixed with the B_4C solution and further sonicated to obtain a uniform mixing of carbon nanofibers and B_4C powders. Finally, the suspension of carbon nanofibers and B_4C powders was infiltrated through a filter paper under a high-pressure compressed air system to make a paper. The as-prepared paper was dried in an oven at 120 °C for 2 h. It has good strength and flexibility to allow for handling like traditional fiber material.

3. Testing of three-layered ceramics

The Young's modulus was measured at room temperature using an impulse excitation method and a Grindo-Sonic MK 5 (Lemmens, Germany). Four point bending strength was measured in the setup with 20 mm loading and 40 mm supporting span. The tests were carried out with a cross-head displacement speed of 1 mm/min at room temperature using the Universal Testing Machine (UPM-Zwick 1478, Germany) in accordance to EN 843-1 [11].

Fracture toughness was measured using the single edge V notch beam (SEVNB) method [12]. The notches of different length were inserted using a notching machine where the final notching was made using 1 μm diamond paste and a steel razor blade [12]. The cross-head displacement speed of 0.3 mm/min was used for measurements at room temperature (USM, Zwick Z005, Germany). Outer and inner support spans of the four-point bending fixture for SEVNB samples were 40 mm and 20 mm, respectively. Specimens with different notches (0.2, 0.4, 0.6, 0.8, 1, 1.2, 1.4, and 2 mm) were tested. Fractographic analysis by scanning electron microscopy (SEM) was carried out on the selected specimens using a Hitachi S-4700 field emission scanning electron microscope.

4. Results and discussion

4.1. Effective Young's moduli of the B_4C/B_4C–$C_{nanofibers}$ laminates

The effective Young's modulus of the three-layered B_4C/B_4C–$C_{nanofibers}$ composite was measured using flexural vibrations of the sample with directions of vibrations shown schematically in Fig. 1. The flexural vibrations of the sample were investigated in two orthogonal directions. The Young's modulus for the longitudinal direction (Fig. 1A) was measured to be 453 ± 3 GPa, which is close to the measured 455 ± 8 GPa value of Young's modulus for pure B_4C. The similar values of effective Young's modulus of a three-layered laminate vibrated in the longitudinal direction along the interfaces between layers and Young's modulus of pure B_4C can be explained assuming an isostrain state in the laminate. The interfacial bonding between the layers is considered to be good and allows for the deformation of different layers to be the same. In this case the effective Young's modulus of the composite in the longitudinal

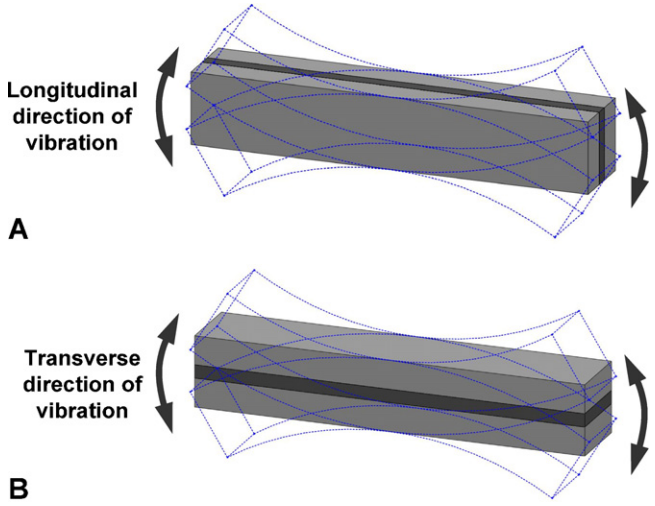

Fig. 1. Directions of flexural vibrations of layered specimen: (A) longitudinal direction of vibration; (B) transverse direction of vibration.

direction can be calculated as

$$E_l = E_1 f_1 + E_2 f_2,$$

where E_1 is the Young's modulus of pure B_4C; f_1 is the volume fraction of B_4C layers in the laminate; E_2 is the Young's modulus of B_4C–$C_{nanofibers}$ layer; f_2 is the volume fraction of B_4C–$C_{nanofibers}$ layer in the laminate. The layered specimens had thick outer layers of B_4C with a thickness of $t_1 = 2625 \pm 110$ μm and a thin central layer of B_4C–$C_{nanofibers}$ with a thickness of $t_2 = 90 \pm 10$ μm. Therefore, the volume fractions of B_4C layers and B_4C–$C_{nanofibers}$ layer in the laminate were 0.983 ± 0.003 and 0.017 ± 0.003, respectively. In such a way, the contribution of Young's modulus of B_4C–$C_{nanofibers}$ layer to the effective Young's modulus of the composite in the longitudinal direction was negligible.

However, there was a significant difference in the effective Young's modulus of the three-layered composite measured in the transverse direction (Fig. 1B), which was equal to 237 ± 105 GPa, in comparison to the values measured both for the three-layered composite in the longitudinal direction and pure B_4C. Such a big difference in measured values can be explained assuming an isostress state, where the stress that the composite is exposed to is the same for the three separate layers. The effective Young's modulus of the composite in a transverse direction can then be calculated as

$$\frac{1}{E_t} = \frac{f_1}{E_1} + \frac{f_2}{E_2}$$

which can be reduced to

$$E_t = \frac{E_1 E_2}{E_1 f_1 + E_2 f_2}.$$

This shows there is a strong contribution of the Young's modulus of the B_4C–$C_{nanofibers}$ layer to the effective Young's modulus of the composite vibrated in the transverse direction. Since Young's modulus of the B_4C–$C_{nanofibers}$ layer is essentially lower than that of the pure dense B_4C layer, the much lower Young's modulus values of the three-layered composite were measured. Additionally, the huge scattering of the measured values of the transverse Young's modulus has been observed because of the presence of microcracks, pores, and other defects, both along the interfaces between B_4C and B_4C–$C_{nanofibers}$ layers and inside B_4C–$C_{nanofibers}$ material (Fig. 2). There are a large number of microcracks and pores in the central B_4C–$C_{nanofibers}$ layer. These defects can significantly affect the elastic modulus of the layer. It results in the large variation of the elastic modulus of the B_4C–$C_{nanofibers}$ layer, therefore, in the large variation of the effective Young's modulus of the composite vibrated in the transverse direction. Therefore, the significant difference between the effective Young's moduli measured in the orthogonal directions of the laminates was detected. The experimental results above allow estimating the elastic modulus of the B_4C–$C_{nanofibers}$ layer as 383 GPa as the first approximation to be made.

4.2. Apparent fracture toughness and threshold stress of the B_4C/B_4C–$C_{nanofibers}$ laminates

A weight function analysis was used to estimate the apparent fracture toughness in laminates with residual stresses [9,13–16]. The choice of coordinate system is of great importance to the apparent fracture toughness calculations because of the significant simplification of the procedure. The most appropriate coordinate origin is on the tensile surface of the sample under bending. The geometry of the multilayered material is such that the problem can be reduced to one dimension and that analytically tractable solutions can be used [9,16].

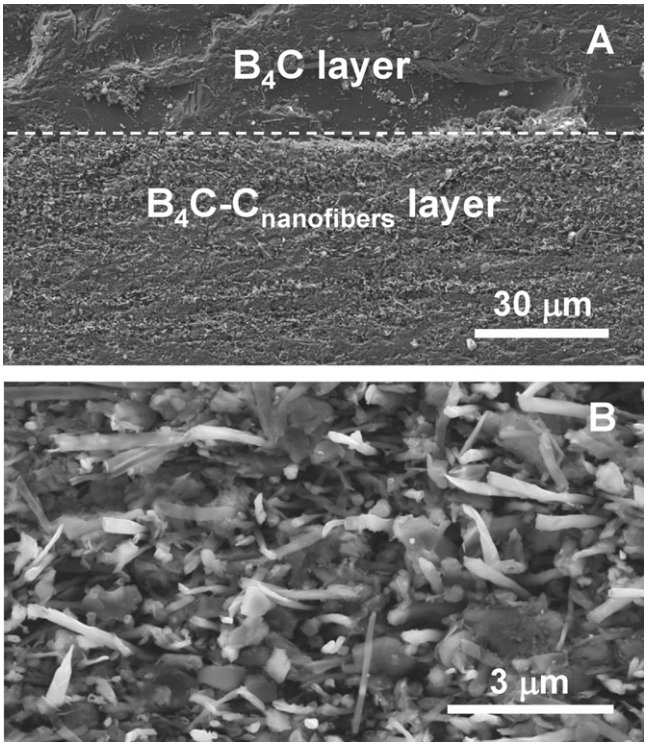

Fig. 2. Micrographs of B_4C/B_4C–$C_{nanofibers}$ layered ceramics. (A) A side view of the bending bar with the interface between B_4C and B_4C–$C_{nanofibers}$ layers; (B) A fracture surface of B_4C–$C_{nanofibers}$ layer.

An experimental value of the apparent fracture toughness can be found using the expression [17]:

$$K_{\text{app}} = Y(\alpha)\sigma_m a^{1/2}, \tag{1}$$

where

$$Y(\alpha) = \frac{1.99 - \alpha(1-\alpha)(2.15 - 3.93\alpha + 2.7\alpha^2)}{(1+2\alpha)(1-\alpha)^{3/2}}, \tag{2}$$

$$\sigma_m = \frac{1.5P(s_1 - s_2)}{bw^2} \quad \text{and } \alpha = a/w, \tag{3}$$

where w is the total thickness of the specimen, P is the critical load (the applied bending load corresponding to specimen failure), a is the crack length, and s_1 and s_2 are outer and inner support spans of the four-point bending fixture for SEVNB samples. Note that in our case of the symmetrical three-layered composite $w = 2t_1 + t_2$.

The apparent fracture toughness of the layered composite for the crack tip located in ith layer can be calculated analytically by [9,16]:

$$K_{\text{app}}^{(i)} = \frac{6Y(\alpha)a^{1/2}(I_{L1}^2 - I_{L0}I_{L2})(K_{1c}^{(i)} - K_r)}{w^2\left\{E'_{n+1}\int_{x_n}^{a} h(x/a,\alpha)[I_{L0}x - I_{L1}]dx + \sum_{i=1}^{n} E'_i \int_{x_{i-1}}^{x_i} h(x/a,\alpha)[I_{L0}x - I_{L1}]dx\right\}}, \tag{4}$$

where $K_{1c}^{(i)}$ is the intrinsic fracture toughness of the ith layer material, K_r is the stress intensity due to the residual stresses $\sigma_r^{(i)}(x)$:

$$K_r = \int_{x_n}^{a} h(x/a,\alpha)\sigma_r^{(n+1)}(x)dx + \sum_{i=1}^{n}\int_{x_{i-1}}^{x_i} h(x/a,\alpha)\sigma_r^{(i)}(x)dx, \tag{5}$$

$$\sigma_r^{(i)}(x) = \frac{E'_i}{I_{L1}^2 - I_{L0}I_{L2}}[I_{L1}J_{L1} - I_{L2}J_{L0} + (I_{L1}J_{L0} - I_{L0}J_{L1})x - \tilde{\varepsilon}_i(I_{L1}^2 - I_{L0}I_{L2})], \tag{6}$$

where $h(x/a, \alpha)$ is the weight function for an edgecracked sample [14–16], x_i is the coordinate of interface between ith and $(i+1)$th layers, $E'_i = E_i/(1-\nu_i)$, and E_i and ν_i are the elastic modulus and Poisson ratio of the ith layer, respectively.

The expressions for I_{Lj} $(j = 0, 1, 2)$ and J_{Lj} $(j = 0, 1)$ were obtained in [16] as follows:

$$I_{Lj} = \frac{1}{j+1}\sum_{i=1}^{N} E'_i(x_i^{j+1} - x_{i-1}^{j+1}), \tag{7}$$

$$J_{Lj} = \frac{1}{j+1}\sum_{i=1}^{N} \tilde{\varepsilon}_i E'_i(x_i^{j+1} - x_{i-1}^{j+1}), \tag{8}$$

where $\tilde{\varepsilon}_i$ is the strain in the ith layer, which is associated with thermal expansion:

$$\tilde{\varepsilon}_i = \int_{T_0}^{T_j} \beta_i(T)dT, \tag{9}$$

where $\beta_i(T)$ is the thermal expansion coefficient of the ith layer at the temperature T. T_0 and T_j are the actual and ''joining'' temperatures, respectively. At a certain temperature T_j, the different components become bonded together and residual stresses appear. In our case, this temperature is equal to the hot pressing temperature of 2150 °C. The linear approximation of $\beta_i(T)$ can be used as a first approximation. Then, $\tilde{\varepsilon}_i = \langle\beta_i\rangle\Delta T$, where $\Delta T = T_j - T_0$, $\langle\beta_i\rangle = (\beta_i(T_0) + \beta_i(T_j)/2)$ is the average value of the thermal expansion coefficient in the temperature range from T_0 to T_j.

The specimens analyzed in the paper are made of three layers only. It is of interest to obtain simplified relations for residual stresses and apparent fracture toughness. In this case the residual stresses in the first and second layers are:

$$\sigma_r^{(1)} = \frac{(\tilde{\varepsilon}_2 - \tilde{\varepsilon}_1)f_2E'_1E'_2}{f_1E'_1 + f_2E'_2} \quad \text{and } \sigma_r^{(2)} = -\frac{f_1}{f_2}\sigma_r^{(1)}. \tag{10}$$

For symmetrical structure, the residual stress acting in the third layer equals to that acting in the first layer. The simplified expressions for the apparent fracture toughness of the three-layered composite are as follows:

$$K_{\text{app}}^{(1)} = \frac{E^*}{E'_1}(K_{1c}^{(1)} - K_r), \tag{11a}$$

$$K_{\text{app}}^{(2)} = \frac{E^*(K_{1c}^{(2)} - K_r)}{E'_2[1 + ((E'_1 - E'_2)/E'_2)((Y(t_1/w))/(Y(a/w)))\sqrt{t_1/a}]}, \tag{11b}$$

$$K_{\text{app}}^{(3)} = \frac{E^*(K_{1c}^{(1)} - K_r)}{E'_1[1 + ((E'_2 - E'_1)/E'_1)((Y((t_1+t_2)/w)\sqrt{t_1+t_2} - Y(t_1/w)\sqrt{t_1})/(Y(a/w)\sqrt{a}))]}, \tag{11c}$$

where formulae (11a), (11b) and (11c) correspond to the crack tips located in the first, second and third layers, respectively, and $E^* = (f_1^3 + 3f_1f_2)E'_1 + f_2^3E'_2$.

The apparent fracture toughness, K_{app}, in layered specimens can be analyzed as a function of the crack length parameter $\tilde{a}$,

where $\tilde{a} = Y(\alpha)a^{1/2}$ [9]. The crack length parameter $\tilde{a}$ is the most appropriate to demonstrate critical conditions of crack growth. One of the advantages of this parameter is that the stress intensity factor of an edge crack for a fixed value of the applied stress, σ_m, is a straight line from the coordinate origin in the coordinate system $K_{app} - \tilde{a}$. Since $K_1 = \sigma_m\tilde{a}$, the slope of the straight line is the applied stress σ_m. The conditions for unstable crack growth in the internal stress field are as follows [18]: $K_1(\sigma_m, a) = K_{app}(a)$; $dK_1(\sigma_m, a)/da \geq dK_{app}(a)/da$. Using parameter $\tilde{a}$, these conditions become $\sigma_m\tilde{a} = K_{app}(\tilde{a})$ and $\sigma_m \geq dK_{app}(\tilde{a})/d\tilde{a}$, which can be reduced to: $K_{app}(\tilde{a})/\tilde{a} \geq dK_{app}(\tilde{a})/d\tilde{a}$. In this case the applied stress intensity factor becomes higher than the fracture resistance of the material.

The B_4C–$C_{nanofibers}$ material in the three-layered composite is a thin layer with a specific structure attached to the thick B_4C layers. It is impossible, though, to obtain bulk specimen for mechanical testing with a microstructure that is identical to the B_4C–$C_{nanofibers}$ material in the three-layered composite. The test procedure for the characterization of a single layer inside the composite is not available yet. For example, indentation methods are unable to determine the in-plane mechanical properties of the thin middle layer in the three-layered composite. First, unknown residual stresses due to edge effects change the indentation response; second, the specific microstructure does not allow imprints that contain enough microstructural elements for the necessary averaging of properties. In such a way, the characterization of the mechanical properties of the thin middle layer with specific microstructure is a complicated scientific problem. Therefore, Poisson ratio, coefficient of thermal expansion, and intrinsic fracture toughness of the second layer as well as residual stresses and apparent fracture toughness were estimated indirectly.

The dependence of apparent fracture toughness on crack length parameter in the three-layered structure is shown in Fig. 3. The solid line and the solid circles correspond to calculated values and are experimental data, respectively. The calculated values were obtained by adjusting the magnitude of the residual stress to provide the best fit of experimental data using the calculation procedure above. Poisson's ratio and thermal expansion coefficient of pure B_4C were chosen to be 0.17 and $5.6 \times 10^{-6}\,K^{-1}$, respectively [10]. Fracture toughness of pure B_4C was measured to be 3.53 MPa $m^{1/2}$. In the case of crack tip located in the first layer the apparent fracture toughness can be calculated using Eqs. (5) and (11a). Note that Poisson ratio of second layer ν_2 and residual stress in the first layer $\sigma_r^{(1)}$ remains to be unknown parameters. However, one can find such a combination of these parameters to provide the least sum of squared deviations of calculated apparent fracture toughness from corresponding experimental values. In our case, the magnitude of the tensile residual stress was estimated as 11.3 ± 2.5 MPa in the thick B_4C layers and the magnitude of the compressive residual stress in the central thin layer was estimated as 455.7 ± 5 MPa, according to Eq. (10). The Poisson ratio of the second layer ν_2 was estimated as 0.3. The thermal expansion coefficient of the B_4C–$C_{nanofibers}$ layer was estimated as $5.2 \times 10^{-6}\,K^{-1}$ using Eq. (10) and the calculated value of the residual stress. One can see that the apparent fracture toughness decreased when the V-notch length increased in the first layer. At the same time, there is a sharp increase of apparent fracture toughness in the second layer. It was shown earlier that such an increase has resulted in crack arrest in the Si_3N_4-based laminates [9,16]. The apparent fracture toughness decreases again when the crack length parameter increases in the third layer.

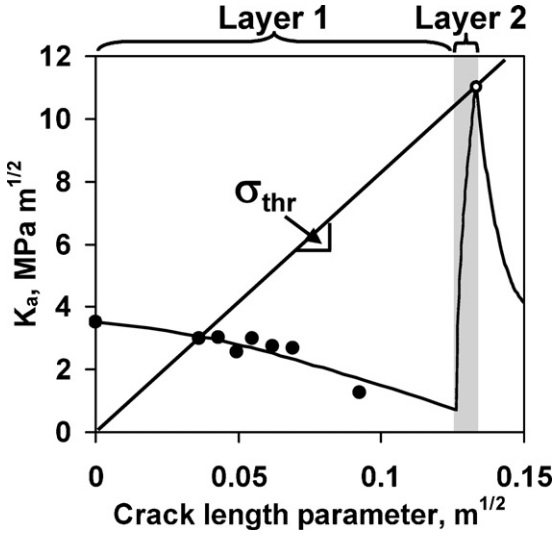

Fig. 3. Dependence of apparent fracture toughness on crack length parameter in three-layered structure.

The stress intensity coefficient of an edge crack for a fixed value of applied stress is depicted in the coordinate system apparent fracture toughness – crack length parameter (Fig. 3) as a straight line from the coordinate origin with slope equal to the applied stress value. The unstable crack growth occurs when the straight line corresponding to the stress intensity factor at constant applied stress will be located above the apparent fracture toughness curve. For edge cracks being inside the first and second layer of our three-layered composite, unstable growth will occur only for stresses corresponding to straight lines, with slope larger than the slope of straight line crossing the apparent fracture toughness maximum. In this case the threshold stress, σ_{thr}, of the laminates is determined by the maximum value of K_{app} at the interface between the second and the third layers (Fig. 3) divided by the corresponding crack length parameter. No failure can occur below this stress if the sample contains the surface cracks located in the first layer.

For our samples, the measured four point bending strength of laminates was equal to 141.6 ± 44.6 MPa with the minimum measured strength of 86 MPa. The minimum strength can be adopted as a threshold stress of the laminate, since no failure occurred below this stress. The obtained value of the threshold stress was used to evaluate the maximum value of apparent fracture toughness, which was found to be about 11 MPa $m^{1/2}$. In turn, this allows the intrinsic fracture toughness of the second layer $K_{1c}^{(2)}$ to be determined as 3.5 MPa $m^{1/2}$.

4.3. Fracture mechanisms of the $B_4C/B_4C–C_{nanofibers}$ laminates

The SEM pictures of the sample tested for fracture toughness are shown in Fig. 4A and B. The schematic of crack development in the three-layered structure with weak interfaces is presented in Fig. 4C. The primary crack propagates in a straightforward manner from the V-notch tip to the interface between the first and second layer. The direction of this propagation is perpendicular to the interface. Note that the primary crack has a small deflection along the interface between the first and second layer then changes its direction. After this, the crack passes through the second layer. The large area of delamination is formed along the interface between the second and third layers. Finally, the secondary crack propagates downward in a straightforward manner from the interface between the second and third layers.

When the stress intensity factor reaches the apparent fracture toughness level for the V-notch tip the unstable growth of the primary crack starts [9]. The crack grows and passes the interface between the first and second layer with high velocity after some acceleration in the first thick layer. Due to the high velocity of propagation, the crack has only a small deflection along the interface between the first and second layer. Then the crack slows to a stop in the second layer due to the increasingly apparent fracture toughness. The unstable growth then changes to stable propagation. The small intact ligament remains between the crack tip and the interface between the second and third layer. The primary crack promotes the development of the interfacial crack along the interface between the second and third layer in this configuration. In this case, the interface between the first and second layer located behind the primary crack tip does not participate in the fracturing process. Then the ligament of the second layer breaks after a large delamination along the interface between the second and third layer [19]. After this, the third layer fails as a separate bending unnotched specimen. Typically, this failure appears at higher loads than the start of the primary crack. In fact, the stress at the start of the secondary crack does not depend on the V-notch length but the strength of the third layer alone.

The typical force-time diagram for the fracture toughness test of the layered specimen is shown in Fig. 5. One can see the linear dependence of the force on time corresponding to elastic behavior of the specimen up to the first maximum force. The maximum corresponds to the primary crack start. This is followed by a force drop due to the decrease of the specimen stiffness resulting from the primary crack propagation. The

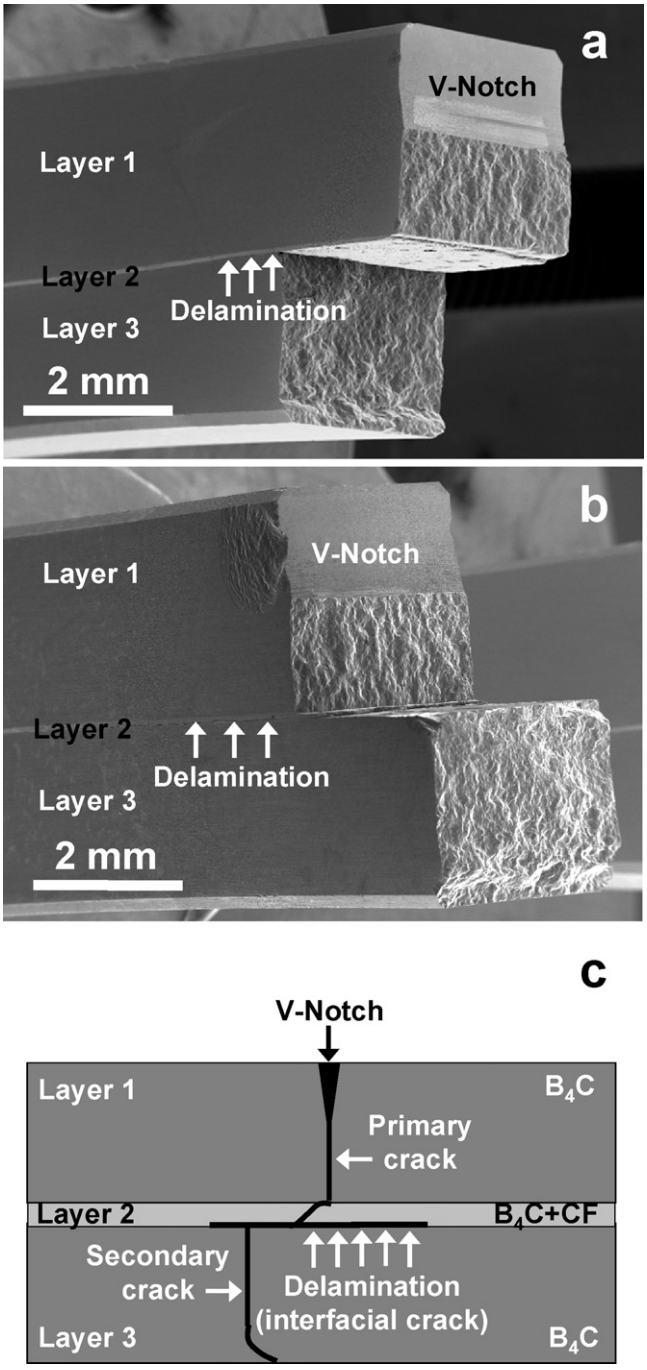

Fig. 4. Failure of the laminate: (A) left part of the sample tested for fracture toughness determination; (B) right part of the sample tested for fracture toughness determination; (C) schematic presentation of crack development in three-layered structure with weak interfaces.

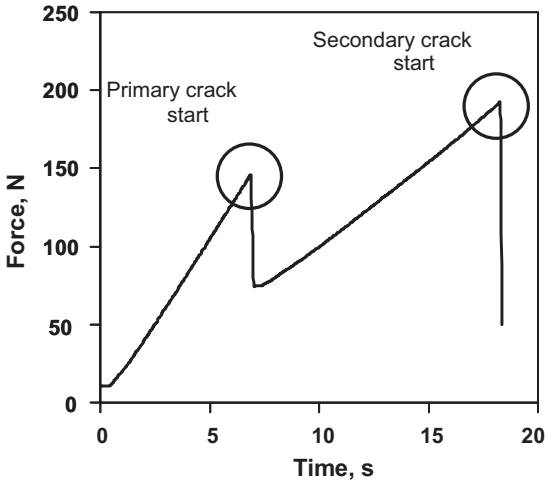

Fig. 5. Typical force–time diagram for fracture toughness test of layered specimen.

almost linear dependence of applied force on time is observed after the force drop. The second maximum corresponds to the secondary crack start. This is followed by the total failure of the specimen.

5. Conclusions

It was shown that a thin layer of B_4C mixed with carbon nanofibers can be used to create a weak interface in a three-layered laminate for crack deflection. The three-layered B_4C/B_4C–70 wt.% $C_{nanofibers}$ laminates were hot pressed at 2100 °C for 1 h at 30 MPa and then tested in four point bending to measure strength and fracture toughness, along with measurements of Young's modulus by a natural frequency technique. The estimation of the thermal residual stresses of the three-layered composite has shown that there should be tensile residual stresses with a magnitude of 11.3 ± 2.5 MPa in an outer pure B_4C layer and 455.7 ± 5 MPa in the inner B_4C–70 wt.% $C_{nanofibers}$ layer. It was established that, indeed, the tensile residual stress in the first outer layer had a significant effect on the apparent fracture toughness of the laminates. For the V-notched samples, the apparent fracture toughness was measured as a function of the notch length. It was established that when the notch length is increased, the apparent fracture toughness decreased when the notch tip was located in the first layer. It was estimated that if the notch tip is placed in the inner layer with a compressive stress, the apparent fracture toughness would go up. Based on the estimation of the apparent fracture toughness the threshold stress of the $B_4C/B_4C–C_{nanofibers}$ laminates was calculated to be equal to 84 MPa.

The crack that originated from the V-notch propagated through the first thick pure B_4C layer then deflected inside of the inner thin $B_4C–C_{nanofibers}$ layer. Next, the delamination occurred along the interface between the thin $B_4C–C_{nanofibers}$ and the still intact B_4C layers. After this, an intact ligament in the central layer between the primary crack and interfacial crack breaks. The secondary crack then starts from the B_4C surface created as a result of delamination. The stress at the start of this crack is not dependent of the V-notch length but determined by the strength of the third layer. As result of the fracture mechanisms acting in the laminates, the gracious failure is observed.

Acknowledgement

This work was supported by NSF projects DMR – 0748364 "CAREER: Hard and tough boron rich ceramic laminates designed to contain thermal residual stresses" and CCMI – 0757302 "Collaborative Research: Development of Multi-functional Nanocomposites with Engineered Carbon Nanopaper".

References

[1] D.-H. Kuo, W.M. Kriven, Fracture of multilayer oxide composites, Mater. Sci. Eng. A241 (1998) 241–250.
[2] R. Bermejo, R. Danzer, High failure resistance layered ceramics using crack bifurcation and interface delamination as reinforcement mechanisms, Eng. Fract. Mech. 77 (2010) 2126–2135.
[3] S. Tariolle, C. Reynaud, F. Thevenot, T. Chartier, J.L. Besson, Preparation, microstructure and mechanical properties of SiC–SiC and $B_4C–B_4C$ laminates, J. Solid State Chem. 177 (2004) 487–492.
[4] H. Tomaszewski, H. Weglarz, A. Wajler, M. Boniecki, D. Kalinski, Multilayer ceramic composites with high failure resistance, J. Eur. Ceram. Soc. 27 (2007) 1373–1377.
[5] W.J. Clegg, K. Kendall, N.McN. Alford, T.W. Button, J.D. Birchall, A simple way to make tough ceramics, Nature 347 (1990) 455–457.
[6] S. Tariolle, F. Thevenot, T. Chartier, J.L. Besson, Properties of reinforced boron carbide laminar composites, J. Eur. Ceram. Soc. 25 (2005) 3639–3647.
[7] W.J. Clegg, Design of ceramic laminates for structural applications, Mater. Sci. Technol. 14 (1998) 483–495.
[8] A.J. Phillipps, W.J. Clegg, T.W. Clyne, Fracture behaviour of ceramic laminates in bending—I. Modelling of crack propagation, Acta Metall. Mater. 41 (1993) 805–817.
[9] M. Lugovy, V. Slyunyayev, N. Orlovskaya, G. Blugan, J. Kuebler, M. Lewis, Apparent fracture toughness of Si_3N_4-based laminates with residual compressive or tensile stresses in surface layers, Acta Mater. 53 (2005) 289–296.
[10] N. Orlovskaya, M. Lugovy, V. Subbotin, A. Radchenko, J. Adams, M. Chheda, J. Shih, J. Sankar, S. Yarmolenko, Robust design and manufacturing of ceramic laminates with controlled thermal residual stresses for enhanced toughness, J. Mater. Sci. 40 (2005) 5483–5490.
[11] European Standard, EN 843-1, Advanced Technical Ceramics−Monolithic Ceramics−General and Textural Properties, Part 1. Determination of flexural strength, 2006.
[12] J. Kuebler, in: J.A. Salem, G.D. Quinn, M.G. Jenkins (Eds.), ASTM STP, 1409, ASTM, 2002, pp. 93–106.
[13] R. Lakshminarayanan, D.K. Shetty, R.A.N. Cutler, Toughening of layered ceramic composites with residual surface compression, J. Am. Ceram. Soc. 79 (1996) 79–87.
[14] R.J. Moon, M. Hoffman, J. Hilden, K. Bowman, K. Trumble, J. Roedel, Weight function analysis on the R-curve behavior of multilayered alumina–zirconia composites, J. Am. Ceram. Soc. 85 (2002) 1505–1511.
[15] T. Fett, D. Munz, Influence of crack-surface interactions on stress intensity factor in ceramics, J. Mater. Sci. Lett. 9 (1990) 1403–1406.
[16] M. Lugovy, V. Slyunyayev, V. Subbotin, N. Orlovskaya, G. Gogotsi, Crack arrest in Si_3N_4-based layered composites with residual stress, Compos. Sci. Technol. 64 (2004) 1947–1957.
[17] J.E. Srawley, Wide range stress intensity factor expressions for ASTM E 399 standard fracture toughness specimens, Int. J. Fract. 12 (1976) 475–476.
[18] V.M. Sglavo, L. Larentis, D.J. Green, Flaw-insensitive ion-exchanged glass: I. Theoretical aspects, J. Am. Ceram. Soc. 84 (2001) 1827–1831.
[19] W. Lee, S.J. Howard, W.J. Clegg, Growth of interface defects and its effect on crack deflection and toughening criteria, Acta Mater. 44 (1996) 3905–3922.